### PVP2023-106333

# PITTING CORROSION RESISTANCE IN THE HEAT-AFFECTED ZONE OF NO-BACKING GAS (NBG) AUSTENITIC STAINLESS STEEL WELDS

Claire Cary<sup>1</sup>, Jorge Penso<sup>2</sup>, Narasi Sridhar<sup>1</sup>, Carolin Fink<sup>1</sup>

<sup>1</sup>Materials Science and Engineering, The Ohio State University, Columbus, OH, United States <sup>2</sup> Shell Global Solutions (US) Inc., Houston, Texas, United States

#### **ABSTRACT**

Stainless steel welds for service applications in corrosive environments are typically performed using gas tungsten arc welding (GTAW) with an inert backing gas in order to minimize or prevent root pass contamination and oxidation. Back purging adds significant cost and complexity to stainless steel pipe welding due to access restrictions, personnel safety, and/or economic factors. In this study, two no-backing gas welds (NBG) were made on Type 304L austenitic stainless steel pipe with Type 316 filler metal. Two different shielding gas mixtures were used (98% Ar-2% CO<sub>2</sub> and 90% He-7.5% Ar-2.5% CO<sub>2</sub>) for the NBG welds. Open gap root pass welds were performed using modified short circuit gas metal arc welding (SC-GMAW) process. A hot pass was welded with pulsed GMAW process. Fill and cap passes were made with flux-cored arc welding (FCAW) process. Cyclic potentiodynamic polarization (CPP) measurements based on ASTM G61 were performed locally on the backside surface heataffected zone as a function of distance from the fusion line. Electrochemical corrosion testing was done using a simple syringe cell setup. Pitting corrosion resistance of the NBG welds was compared to a reference weld made with 100% argon backing gas and conventional GTAW for the root and hot pass.

Keywords: Gas metal arc welding, No backing gas welding, Stainless Steel, Pitting Corrosion

#### **NOMENCLATURE**

AI	Aigon
ArBG	Argon backing gas
$CO_2$	Carbon dioxide

CPP Cyclic potentiodynamic polarization

Epit Pitting potential
Erp Repassivation potential
FCAW Flux cored arc welding
GMAW Gas metal arc welding
GMAW-P Pulsed gas metal arc welding
GTAW Gas tungsten arc welding

HAZ Heat affected zone

He Helium NBG No back

NBG No backing gas PCR Pitting corrosion resistance

SC-GMAW Short circuit gas metal arc welding

## 1. INTRODUCTION

Open gap pipe welds on austenitic stainless steel are currently made using gas tungsten arc welding (GTAW) process with an inert backing gas (typically 100% argon) to minimize oxidation of the root and maintain corrosion resistance on the inner pipe surface. This adds significant cost and complexity to stainless steel pipe welding due to access restrictions, personnel safety, and/or economic factors. No-backing gas (NBG) welding technology using modified short-circuit gas metal arc welding (SC-GMAW) for stainless steel pipe was developed about 20 years ago [1], but has not been widely adopted, in particular for service applications in corrosive environments. Barriers to implementation include a need for qualification overhaul and a lack of information or trust in NBG techniques [2], [3]. Several studies have reported no significant differences in corrosion behavior and mechanical properties of NBG welds on austenitic stainless steels when compared to control welds with argon backing [1, 3–5]. ASME B31.3/IX Codes acceptable NBG welds were made utilizing advanced/modified SC-GMAW processes for welding the root pass and Si-rich filler metals to improve oxidation immunity and fluidity of the weld metal.

Different shielding gas options are available for GMAW of austenitic stainless steel; the use of helium in the shielding gas makes the process typically very expensive. *Rajan et al.* [5] reported that the use of argon-based shielding gas mixtures for no-backing gas GMAW on austenitic stainless steel Type 304/304L provided acceptable weld appearance, weld quality and mechanical properties. There were no significant differences in corrosion weight loss in ASTM G48 Method A [7] when compared to an NBG weld made with a high helium tri-mix

shielding gas, and to a reference GTAW welds made with 100% argon backing gas.

In this study, we characterized the corrosion resistance of no-backing gas GMAW welds on Type 304L stainless steel pipe using ER316LSi filler wire. Cyclic potentiodynamic polarization (CPP) measurements based on ASTM G61 were performed locally on the backside surface heat-affected zone (HAZ), i.e. the inner pipe surface that would be subjected to the corrosive environment. The pitting corrosion behavior in the backside HAZ of the NBG welds was compared to results from a reference weld made with GTAW process and 100% argon backing gas. In addition, the used syringe cell setup enabled the characterization of changes in pitting corrosion resistance in different regions of the HAZ, i.e. as a function of distance from the root. Two different shielding gas mixtures were used for the NBG welds (98% Ar-2% CO<sub>2</sub> and 90% He-7.5% Ar-2.5% CO<sub>2</sub>) to study the effect on the oxidation behavior of the root and HAZ for these kind of no-backing gas welds. In summary, the objective of this study was to analyze how the use of different shielding gases in no-backing gas GMAW of austenitic stainless steel influences weld root oxidation, overall pitting corrosion resistance in the backside HAZ, and corrosion behavior locally in different regions of the HAZ.

#### 2. MATERIALS AND METHODS

Welds were made on Type 304L austenitic stainless steel pipe (14 in. diameter) with a thickness of 12.7 mm (1/2 in.). The joint geometry is shown in Figure 1. Three welds were made for this study as summarized in Table 1. Two no-backing gas (NBG) welds were made with ER316LSi filler wire (AWS A5.9/A5.9 M [8]) using modified short-circuit gas metal arc welding (SC-GMAW) for the root pass, and pulsed GMAW for the hot pass weld. Two different shielding gas mixtures were used (98% Ar/2% CO<sub>2</sub> and 90% He, 7.5% Ar, 2.5% CO<sub>2</sub>) for the NBG welds. The fill and cap passes were welded with FCAW process using E316LT1-4 electrode. A reference weld was made with 100% argon backing and GTAW process for the root and hot pass using ER316L. The combined thickness of the root and hot pass was 6 mm for all welds. The fill and cap passes of the reference weld were also made using FCAW and E316LT1-4. Heat input for root, hot and fill and cap passes are provided in Table 1.

Electrochemical corrosion testing was done locally on the root side of the welds in the heat affected zone (HAZ) (i.e., the inner surface of the pipe which would be subjected to the corrosive environment). In order to discern possible changes in behavior across HAZ regions, a small test area is needed, which can be achieved using a syringe cell setup, where only a droplet-sized area is subjected to the solution during testing. This method was first proposed by Panindre et al. [9]. The exposed area is defined by a hanging droplet between the syringe cell tip and the test surface by forces of adhesion and cohesion. This approach also combats crevice corrosion, which is often encountered in austenitic stainless steel in particular when using immersion testing. The syringe cell setup used in this study is shown in Figure 2. The approximate exposed area using a 50 mL syringe

was 0.13-0.20 cm<sup>2</sup>. The other components of the system, including the platinum wire counter electrode, Ag/AgCl reference electrode, and test solution, were housed inside the syringe in an aerated, sealed system.

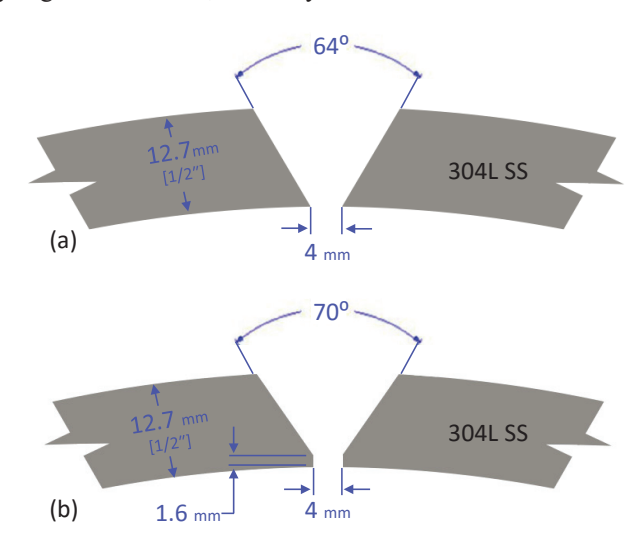


**Figure 1:** Joint geometry for (a) the no-backing gas (NBG) welds using SC-GMAW and GMAW-P for root and hot pass, respectively; and (b) the reference weld with argon backing using GTAW for both, the root and hot pass. Fill and cap passes were made with FCAW for all welds.

**Table 1:** Summary of welding conditions for no-backing gas (NBG) welds and argon backing gas (ArBG) reference weld.

	NBG #1	NBG #2	ArBG
Base metal	ASME SA-312 304L (12.7 mm)		
Backing gas	None		100% Argon
Shielding gas	98% Ar, 2% CO <sub>2</sub>	90% He, 7.5% Ar, 2.5% CO <sub>2</sub>	100% Argon
Root pass welding process	SC-GMAW		GTAW
Hot pass welding process	GMAW-P		GTAW
Fill and cap welding process	FCAW		
Filler metal (root and hot pass)	ER316LSi		ER316L
Filler metal (fill and cap passes)	E316LT1-4		
Heat input (root pass)	0.73 kJ/mm	0.84 kJ/mm	0.89 kJ/mm
Heat input (hot pass)	1.37 kJ/mm	0.98 kJ/mm	0.79 kJ/mm
Heat input (fill and cap passes)	1.67 kJ/mm	1.55 kJ/mm	1.43 kJ/mm

For this work, cyclic potentiodynamic polarization (CPP) electrochemical testing was performed based on ASTM G61 [10] This test provides information about the resistance to localized pitting corrosion of the work piece, most notably providing the pitting potential ( $E_{pit}$ ) and the repassivation potential ( $E_{rp}$ ) of the

test area. Testing was performed in 0.1 M NaCl solution aerated in the syringe using deionized water. Testing was done at room temperature. CPP curves were obtained using a potentiostat (Gamry Instruments) starting with an open circuit potential ( $E_{\rm oc}$ ) measurement for 100 s. The potential was then stepped up at a scan rate of 1.0 mV/s from -0.2 V below the open circuit potential. The potential scan direction was reversed when 0.1 mA/cm² was reached, and the potential was stepped down to -0.2 V below the open circuit potential.

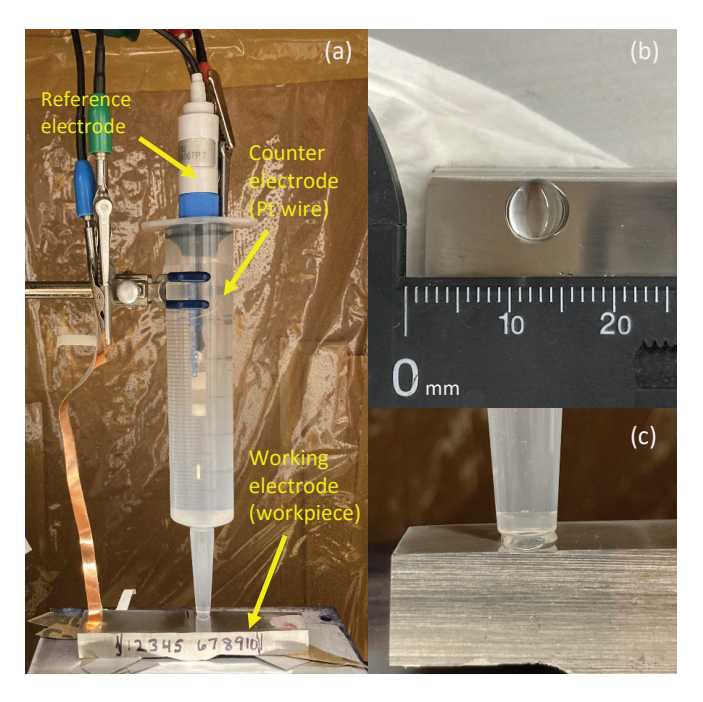


**Figure 2:** Syringe cell setup for cyclic potentiodynamic polarization (CPP) electrochemical corrosion test: (a) overall setup, (b) illustrating droplet size that defines exposed area, and (c) actual droplet between syringe tip and metal surface during testing.

Certain deviations were made from ASTM G61, including the use of a weaker solution concentration, a shorter open circuit potential duration, and a faster scan rate. These concessions were made to preserve the droplet size during testing and increase the sensitivity of the results. Droplet shrinkage is a common challenge when performing syringe cell testing, and a faster scan rate and shorter open circuit duration alleviates competition against evaporation of the droplet. Containing the testing to a humidity chamber also improved droplet shrinkage. Humidity was maintained at a minimum of 60% as measured using a humidity meter. A weaker solution of 0.1 M NaCl (compared to 0.6 M NaCl) can lead to improved sensitivity of the obtained pitting potential and repassivation potential, because increased solution concentration causes more harsh corrosive attack on the work piece that blurs the propensity for pitting corrosion resistance. Lower Cl- concentrations can also help distinguish small differences in pitting behavior between the different welds in this study and is particularly important in analysis across the HAZ.

CPP measurements were made in five zones in the backside surface HAZ of each weld, starting adjacent to the fusion line and following consecutively along the HAZ away from the weld root. Five curves were obtained in each zone for the three welds tested in this study. A schematic of the test locations (zones) in the HAZ can be seen in Figure 3. Prior to testing, the HAZ was mechanically ground with SiC papers to 600 grit followed by an ethanol rinse and dried in hot air to expose a fresh surface. Testing on the heat-tinted (as-welded) HAZ did not yield repeatable curves.

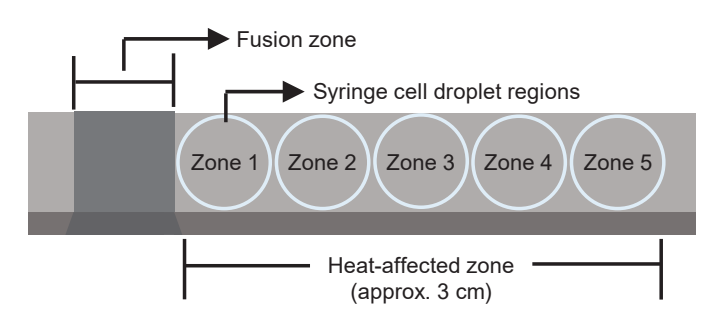


**Figure 3:** Schematic of syringe cell droplets placed in the HAZ as a function of distance from the fusion line. Each zone tested was 0.13- $0.20~\rm cm^2$  (i.e. droplet diameter  $\sim 0.5~\rm cm$ ) as defined by the size of the hanging droplet. Five CPP curves were obtained from each zone.

The critical pitting potential (E<sub>pit</sub>) is the potential above which stable pits initiate rapidly. The repassivation potential (E<sub>rp</sub>) is the potential below which stable pits cease to grow. Both values were determined from the obtained CPP curves. Figure 4 shows a schematic of a typical CPP curve with positive hysteresis loop and the associated values for the pitting and repassivation potential. Epit was determined from the breakdown potential, which is indicated by a sharp increase in current density as the potential is stepped up during the test. As the potential scan direction is reversed, repassivation occurs towards E<sub>rp</sub>, which was determined in this study from the static point potential at 1.0E-6 A/cm<sup>2</sup> current density once a full positive hysteresis loop was complete. In general, the pitting potential is more sensitive to microstructure and surface conditions than the repassivation potential. However, localized corrosion can occur at potentials lower than the pitting potential, so that the pitting potential is not a conservative measure for long-term performance prediction. The repassivation potential has been shown to be a better indicator of long-term pitting performance [11], [12]. Another indicator for pitting corrosion performance used in this study is the probability for low pitting corrosion resistance (PCR), which is defined as the potential difference between E<sub>pit</sub> and E<sub>rp</sub> [13]. If the difference between E<sub>pit</sub> and E<sub>rp</sub> is larger, than there is a higher probability of low corrosion resistance, because it takes more potential to recover the passive layer.

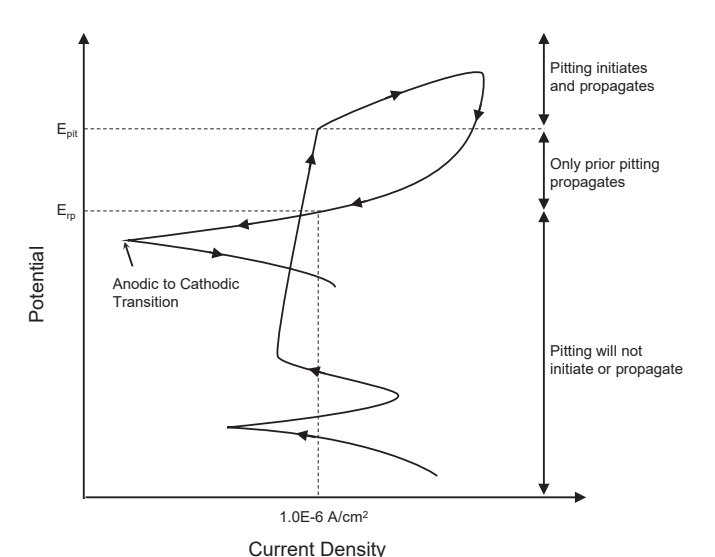


**Figure 4:** Schematic of CPP curve with positive hysteresis loop and associated values of pitting potential and repassivation potential. Adapted from [13].

Pitting morphology in the root side HAZ was captured directly after CPP testing using optical light microscopy. In addition, plane view sections from the root side HAZ were prepared to capture the HAZ microstructure in the CPP test locations (refer to Figure 3). Samples were ground and polished to  $1\,\mu m$  using microdiamond suspension, and then etched electrolytically using 10% oxalic acid at 10~V for 40~s.

#### 3. RESULTS AND DISCUSSION

#### 3.1 Weld backside appearance

Figure 5 illustrates the backside surface appearance of all three weld. The argon backing reference weld (Figure 5c) had little to no oxidation on the root bead and a smooth, rounded appearance. The no-backing gas (NBG) welds showed distinct differences in root bread shape and root bead oxidation of varying degree. The NBG weld with 98% Ar-2% CO<sub>2</sub> shielding gas (Figure 5a) showed a similar rounded root bead shape as the argon backing reference weld, but had a highly textured surface with some oxidation and slightly jagged edges. Some amount of spatter could be seen in the heat-affected zone (HAZ). The NBG weld with tri-mix shielding gas (90% He-7.5% Ar-2.5% CO<sub>2</sub>) (Figure 5b) showed a nearly completely oxidized root bead that was almost plane with the base metal. A thin, raised lip could be seen on either edge of the root. The higher level of root oxidation with the tri-mix shielding gas may be related to the increased arc voltage when using He-based shielding gas resulting in a hotter arc and root weld metal that is exposed to the atmosphere on the backside weld surface. Argon mixtures are reported to create a cleaner weld surface. In addition, helium mixtures would dissipate away from root because of their density being lighter than air, while argon mixtures would fall towards the leading edge/root and provide some protection from oxidation [14].

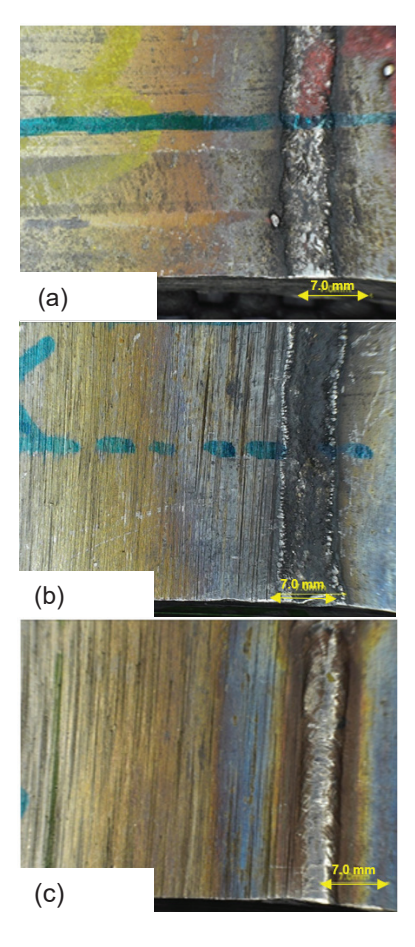


**Figure 5:** Weld backside surface appearance of (a, b) the no-backing gas welds (NBG) with modified short-circuit GMAW process for the root and hot pass welds: (a) using 98% Ar-2% CO<sub>2</sub> shielding gas, and (b) using 90% He-7.5% Ar-2.5% CO<sub>2</sub> shielding gas; and (c) of the reference weld with 100% argon backing using GTAW for the root and hot pass welds.

A simple eye test following visual guidance provided in AWS D18.1/D18.1 M [15] was used to determine the degree of discoloration in the HAZ of the NBG welds and the reference weld with 100% argon backing. Each weld showed a distinct heat tint oxidation appearance in the HAZ. From the fusion line of the root bead outward, the argon backing reference weld (Figure 5c) exhibited a brown region followed by a thin yellow region, then blue, orange and then a much wider yellow region into the unaffected base metal. The NBG weld with 98% Ar-2% CO<sub>2</sub> shielding gas (Figure 5a) exhibited a black region, followed by a grey region, then blue, distinct orange, and a vellow region into the unaffected base metal. Finally, the NBG weld with tri-mix shielding (90% He-7.5% Ar-2.5% CO<sub>2</sub>) (Figure 5b) showed a similar black region, then grey, blue, orange, and yellow. The width of the grey-blue region is significantly wider compared to the NBG weld with argon mixture shielding (Figure 5a). Again, this may be related to the hotter arc when using He-based shielding gas.

#### 3.2 Pitting corrosion resistance

Figure 6 shows representative cyclic potentiodynamic polarization (CPP) curves obtained in 0.1 M NaCl solution from the backside heat-affected zone (HAZ) of the NBG welds and the argon backing reference weld. All curves obtained from the test welds exhibited a positive hysteresis loop (i.e., the reverse scan current is higher than the forward scan current) associated with pitting corrosion. Metastable pits that initiate and terminate prior to pit propagation can be seen by sharp and temporary increases in current density below the pitting potential (Figure 6). The pitting potential ( $E_{pit}$ ) and the repassivation potential ( $E_{rp}$ ) were obtained from each curve. The probability for low pitting corrosion resistance (PCR) was calculated as the difference between  $E_{pit}$  and  $E_{rp}$ .

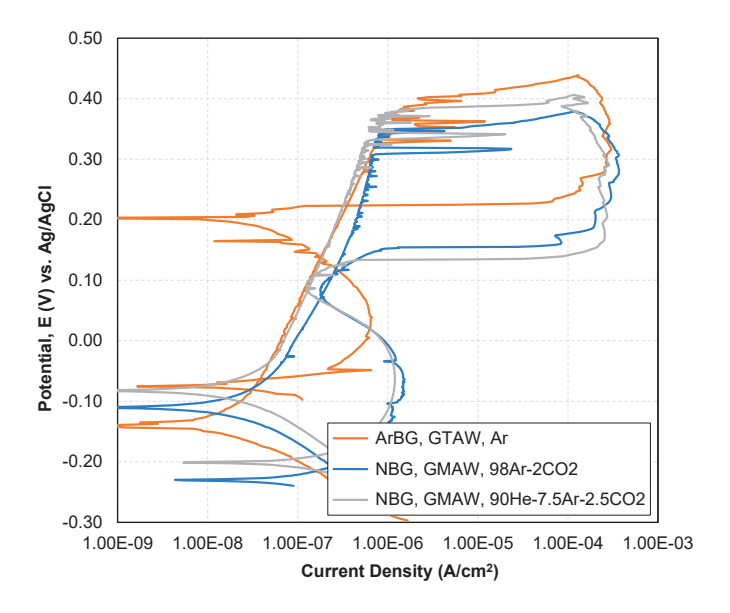


**Figure 6:** Representative CPP curves obtained in the heat-affected zone of the two no-backing gas (NBG) welds, and the reference weld with 100% argon backing.

An evaluation of the overall pitting corrosion resistance in the HAZ was done by averaging the pitting potential and repassivation potential obtained from all test locations (zones) in the HAZ (see Figure 3). Table 2 summarizes the average values and corresponding standard deviations across all CPP curves obtained from the HAZ of the NBG welds and the argon backing reference weld. The pitting potential in the HAZ of the two NBG welds was similar;  $367 \pm 39$  with 98% Ar-2% CO<sub>2</sub> shielding gas, and  $370 \pm 45$  with tri-mix shielding gas (90% He-7.5% Ar-2.5% CO<sub>2</sub>). The argon backing gas reference weld achieved a slightly higher average  $E_{pit}$  of  $376 \pm 48$ . Differences between the test welds were larger in terms of repassivation potential, but all values were within the standard deviation. The lowest E<sub>rp</sub>  $(140 \pm 64)$  was obtained for the NBG weld with helium mixture shielding gas. The NBG weld with argon mixture shielding achieved an  $E_{rp}$  of 152  $\pm$  75. The highest  $E_{rp}$  was obtained for the argon backing reference weld ( $164 \pm 89$ ). Based on these average values for pitting potential and repassivation potential

across all of the HAZ, the NBG weld with tri-mix shielding gas (90% He-7.5% Ar-2.5% CO<sub>2</sub>) showed the highest probability for low corrosion resistance (PCR of 230  $\pm$  67). The PCR for the NBG weld with 98% Ar-2% CO<sub>2</sub> shielding gas was lower (215  $\pm$  80), and similar to the argon backing gas reference weld (212  $\pm$  83). Again, all PCR values were well within the standard deviation.

**Table 2:** Pitting potential ( $E_{pit}$ ) and repassivation potential ( $E_{rp}$ ) across all obtained CPP curves from the HAZ of the no-backing gas (NBG) welds and the argon backing gas (ArBG) reference weld. Average values are given with standard deviation. The probability for low pitting corrosion resistance (PCR) is given as difference between  $E_{pit}$  and  $E_{rp}$ .

	NBG #1	NBG #2	ArBG
Backing gas	None		100% Argon
Shielding gas	98% Ar, 2% CO <sub>2</sub>	90% He, 7.5% Ar, 2.5% CO <sub>2</sub>	100% Argon
Root pass welding process	SC-GMAW		GTAW
Hot pass welding process	GMAW-P		GTAW
Pitting potential (E <sub>pit</sub> )	$367 \pm 39$	$370 \pm 45$	$376 \pm 48$
Repassivation potential (E <sub>rp</sub> )	152 ± 75	140 ± 64	164 ± 89
PCR	$215\pm80$	$230 \pm 67$	$212\pm83$

Plotting the pitting potential and repassivation potential obtained from each test location (zone) in the HAZ yielded further insight into the corrosion behavior locally in the HAZ. The data is summarized in Table 3 for reference. Figure 7 shows that  $E_{pit}$  generally increased at larger distance from the fusion line. Note that there were some exceptions to this trend, and the corresponding standard deviation error bars overlap for most of the data points. For the NBG welds with  $98\% Ar-2\% CO_2$  shielding gas, the pitting potential appeared similar across all of the HAZ, with the highest average value obtained very close to the fusion line (zone 1). The argon backing gas reference weld exhibited the lowest average  $E_{pit}$  close to the fusion line (zone 1), but a distinct increase just slightly further into the HAZ (zone 2) was observed.

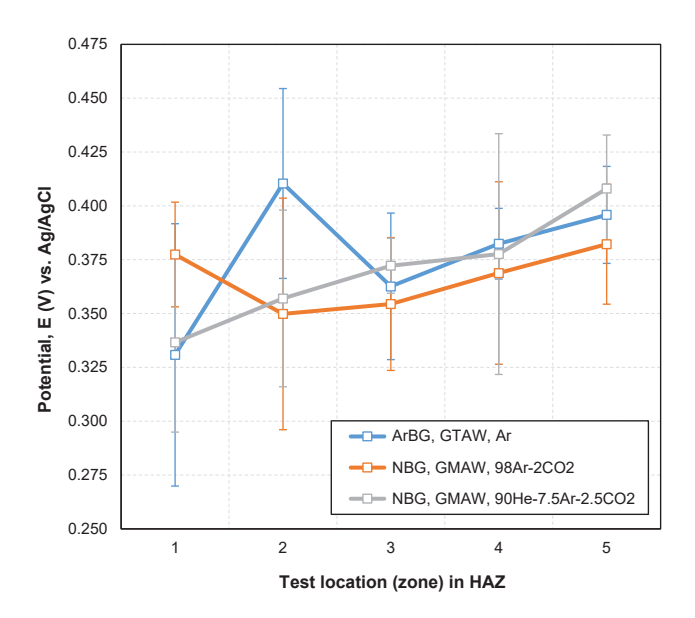
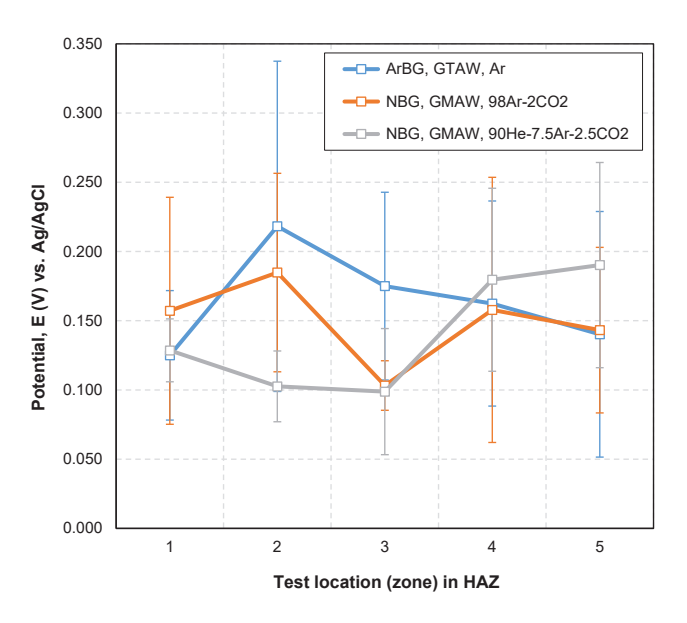


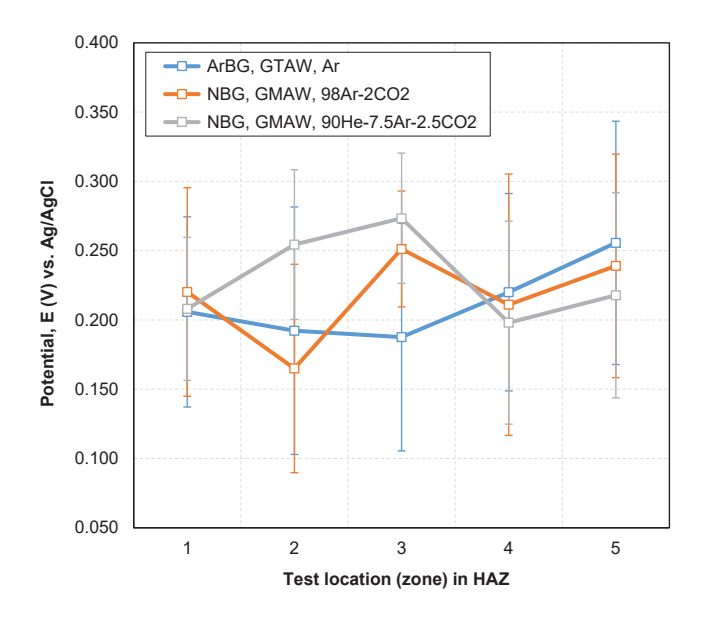
Figure 7: Pitting potential ( $E_{pit}$ ) in the heat-affected zone (HAZ) of the two no-backing gas (NBG) welds, and the reference weld with 100% argon backing.

Figure 8 plots the repassivation potential obtained in the HAZ as a function of distance from the fusion line. The argon backing gas reference weld showed an increase in  $E_{\rm rp}$  in zone 2, similar to what was observed for  $E_{\rm pit}$  (Figure 7). Taking into account the standard deviation, the  $E_{\rm rp}$  was relatively constant further out into the HAZ for the reference weld. For most of the HAZ (i.e. test locations), the NBG welds showed a similar  $E_{\rm rp}$  compared to the argon backing gas reference weld; in particular very close to the fusion line (zone 1), and farthest away from the fusion line (zone 4 and 5). Interestingly, the in-between region (zone 2 and 3) showed lower  $E_{\rm rp}$  values compared to the reference weld, in particular, for the NBG weld with tri-mix shielding gas (90% He-7.5% Ar-2.5% CO<sub>2</sub>). It is hypothesized that this may correspond to the extended grey-blue heat tinted region that was observed for this weld (see Figure 5).

Finally, the calculated probability for low pitting corrosion resistance (PCR) is plotted in Figure 9. It can be seen, that the PCR was very similar between the NBG welds and the argon backing reference welds for most of the HAZ. A higher PCR was observed in zone 2 and 3 for the NBG weld with tri-mix shielding gas (90% He-7.5% Ar-2.5% CO<sub>2</sub>) compared to the argon backing reference weld. The NBG weld with 98%Ar-2%CO<sub>2</sub> shielding gas showed a higher PCR only in zone 3 compared to the argon backing reference weld. The differences in PCR are primarily driven by the observed differences in repassivation potential.



**Figure 8:** Repassivation potential (E<sub>rp</sub>) in the heat-affected zone (HAZ) of the two no-backing gas (NBG) welds, and the reference weld with 100% argon backing.



**Figure 9:** Probability for low pitting corrosion resistance (PCR) in the heat-affected zone (HAZ) of the two no-backing gas (NBG) welds, and the reference weld with 100% argon backing.

**Table 3:** Pitting potential ( $E_{pit}$ ) and repassivation potential ( $E_{rp}$ ) in the HAZ of the no-backing gas (NBG) welds and the argon backing gas (ArBG) reference weld. Data is shown as a function of distance from the fusion line. Average values and standard deviations are given for each test location (zone) in the HAZ. The probability for low pitting corrosion resistance (PCR) is given as difference between  $E_{pit}$  and  $E_{rp}$ .

	NBG #1	NBG #2	ArBG		
Backing gas	No	None			
Shielding gas	98% Ar, 2% CO <sub>2</sub>	90% He, 7.5% Ar, 2.5% CO <sub>2</sub>	100% Argon		
Root pass welding process	SC-G	SC-GMAW			
Hot pass welding process	GMA	AW-P	GTAW		
	Zone	: 1			
Pitting potential (E <sub>pit</sub> )	377 ± 24	337 ± 42	331 ± 61		
Repassivation potential (E <sub>rp</sub> )	157 ± 82	129 ± 23	125 ± 47		
PCR	$220\pm75$	$208 \pm 52$	$206 \pm 69$		
	Zone	: 2			
Pitting potential (E <sub>pit</sub> )	$350 \pm 54$	357 ± 41	410 ± 44		
Repassivation potential (E <sub>rp</sub> )	$185 \pm 72$	103 ± 26	218 ± 119		
PCR	$165 \pm 75$	254 ± 54	192 ± 89		
Zone 3					
Pitting potential (E <sub>pit</sub> )	354 ± 31	372 ± 14	363 ± 34		
Repassivation potential (E <sub>rp</sub> )	103 ± 18	113 ± 40	175 ± 68		
PCR	251 ± 42	$259 \pm 42$	188 ± 82		
Zone 4					
Pitting potential (E <sub>pit</sub> )	$369 \pm 42$	378 ± 56	382 ± 16		
Repassivation potential (E <sub>rp</sub> )	158 ± 96	180 ± 66	162 ± 74		
PCR	211 ± 94	198 ± 73	$220\pm71$		
Zone 5					
Pitting potential (E <sub>pit</sub> )	$382 \pm 28$	408 ± 25	396 ± 23		
Repassivation potential (E <sub>rp</sub> )	143 ± 60	190 ± 74	140 ± 89		
PCR	$239 \pm 81$	218 ± 74	$256 \pm 88$		

#### 3.3 Pitting morphology and HAZ microstructure

Representative images of the pitting morphology in the root side HAZ directly after CPP testing are shown in Figure 10. There were no apparent differences in pitting morphology between the no-backing gas welds and the reference weld. The observed pits on the sample surface appear rounded with variable size and were dispersed over the test area. This is what is typically observed for pitting corrosion.

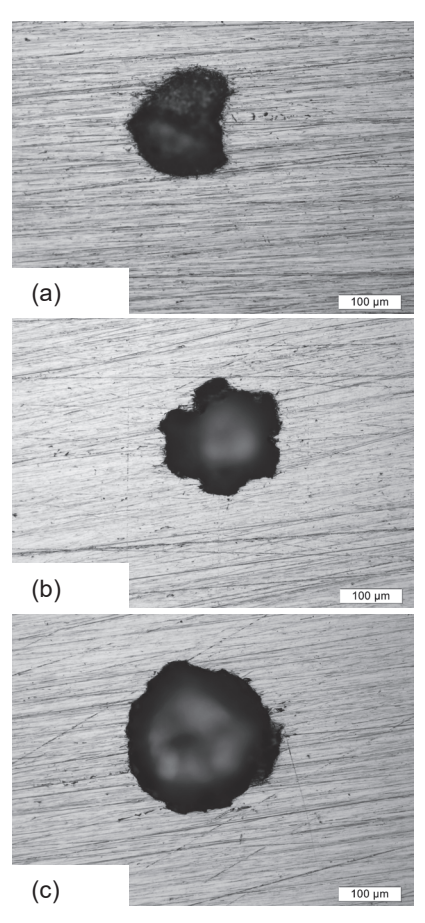


**Figure 10:** Light optical images of pitting morphology directly following CPP testing in the root side HAZ in the (a) reference weld with 100% argon backing gas (ArBG), (b) no-backing gas weld with 90% He-7.5% Ar-2.5% CO<sub>2</sub> shielding gas (NBG #2), and (c) no-backing gas weld with 98% Ar-2% CO<sub>2</sub> shielding gas (NBG #1).

Using optical light microscopy, the microstructure in the polished and etched root side HAZ appears fully austenitic for all welds. Figure 11 shows representative micrographs for the no-backing gas weld with tri mixture shielding (90% He-7.5%Ar-2.5% CO<sub>2</sub>). No differences were observed in terms of the HAZ microstructure between the no-backing gas welds and the reference weld, or as a function of distance from the fusion boundary, i.e. in the different test locations (zones) in the HAZ. Carbides were visible in the grain interiors as black speckles and some coarser nitrides or carbonitrides were observed. Carbides

are likely also present along grain boundaries. However, the latter are too small in size to be resolved with optical light microscopy. No noticeable grain growth was observed close to the fusion boundary, which is another indication that grain boundary carbides were present and effectively pinned grain boundaries upon high temperature exposure in the HAZ. Higher resolution microscopy would be needed to explore subtle differences in secondary phases, morphology and distribution between the welds and as a function of distance from the fusion boundary.

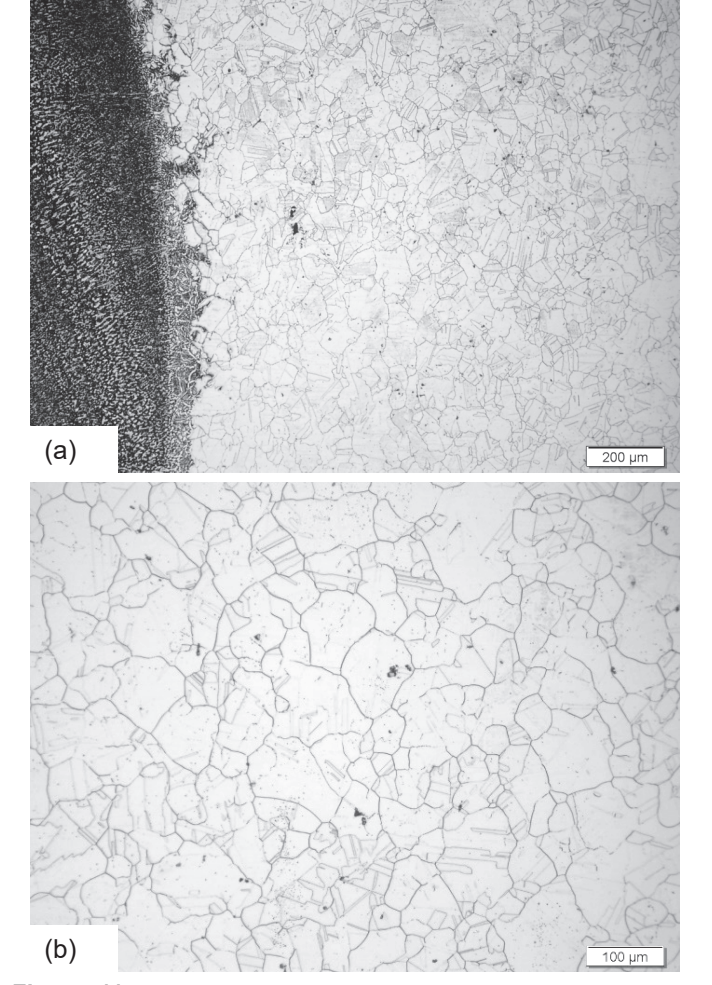


**Figure 11:** Light optical images of plane view sections from the polished and etched HAZ microstructure of the no-backing gas weld with 90% He-7.5% Ar-2.5% CO<sub>2</sub> shielding gas: (a) regions immediately adjacent to the fusion boundary (part of zone 1), and (b) regions further away from the fusion boundary (part of zone 4). No differences in microstructure were observed between no-backing gas welds and the reference welds, or as a function of distance from the fusion boundary.

#### 4. CONCLUSION

The results of this study indicate that no-backing gas (NBG) gas metal arc welding (GMAW) of austenitic stainless steel shows promise as a viable technique to achieve corrosion

resistant welds competitive with gas tungsten arc welding (GTAW) with argon backing gas.

The type of shielding gas used for the NBG welds significantly influenced root shape and degree of oxidation. Argon mixture shielding (98% Ar-2% CO<sub>2</sub>) produced a more rounded root bead with less oxidation compared to the weld made with helium mixture shielding gas (90% He-7.5%Ar-2.5% CO<sub>2</sub>). Differences were also seen in the heat tint oxidation in the backside heat-affected zone (HAZ). The helium mixture shielding produced a wider grey-blue heat tint region compared to the NBG weld with argon mixture shielding and the argon backing gas GTAW reference weld.

Overall, there were no significant differences in pitting corrosion resistance of the backside HAZ between the NBG welds and the argon backing gas reference weld. Corrosion testing in different regions of the backside HAZ (i.e., as function of distance from the root) revealed that there may be small differences locally in corrosion behavior. Further analysis of the heat tint oxidation of the NBG welds is ongoing and expected to provide some insight into what is driving these local differences. In addition, immersion testing following ASTM G48 Method A is planned in the future to compare pitting morphology, location and density to what was observed in cyclic potentiodynamic polarization (CPP) testing in this work.

#### **ACKNOWLEDGEMENTS**

The authors gratefully acknowledge support from Shell and Fluor for preparation of the welded samples. Corrosion testing was performed at the Fontana Corrosion Center at The Ohio State University.

Financial support was provided by the Manufacturing & Materials Joining Innovation Center (Ma²JIC), made possible through an award (2052747) from the National Science Foundation Industry University Cooperative Research Center Program (IUCRC), including supplemental funding through an REV award for undergraduate veteran student support, and through the high school student internship program.

#### **REFERENCES**

- [1] B. Messer, G. Lawrence, V. Oprea, C. Patrick, and T. Phillips, "Welding stainless steel piping with no backing gas," *Welding Journal*, vol. 81, no. 12, pp. 32–34, 2002.
- [2] S. K. Chiluvuri, K. Bliss, and J. Penso, "Evaluation of Welding Techniques for Stainless Steels Piping Without Use of Backing Gas," in *Volume 6B: Materials and Fabrication*, San Antonio, Texas, USA, Jul. 2019, p. V06BT06A004. doi: 10.1115/PVP2019-93359.
- [3] C. Sanagavaram, S. Chiluvuri, and J. Penso, "Evaluation of Welding Techniques for Stainless Steel Piping Without Use of Backing Gas," in *Proceedings of the ASME 2022 Pressure Vessels & Piping Conference*, Las Vegas, NV, United States, Jul. 2022.
- [4] B. Messer, S. Seitz, C. Patrick, and K. Armstrong, "A Novel Technological Assessment for Welding Heavy Wall Stainless Steel," in *Proceedings of the ASME Pressure*

- Vessel and Piping Conference, Jul. 2005, vol. 6, pp. 527–533.
- [5] V. Rajan, B. Narayanan, M. Barrett, and K. Beardsley, "Stainless Steel Pipe Welding With No Backing Gas," in *Proceedings of the ASME 2020 Pressure Vessels & Piping Conference*, Minneapolis, Minnesota, USA, Jul. 2020.
- [6] J. McNicol, B. Narayanan, N. Sridhar, and C. Fink, "Corrosion resistance of austenitic stainless steel welds with no-backing gas," *Weld World*, Dec. 2022, doi: 10.1007/s40194-022-01442-x.
- [7] "ASTM G48-11 (Reapproved 2020), Standard Test Methods for Pitting and Crevice Corrosion Resistance of Stainless Steels and Related Alloys by Use of Ferric Chloride Solution." ASTM International, 2020.
- [8] "AWS A5.9/A5.9M:2006 Specification for Bare Stainless Steel Welding Electrodes and Rods." AWS, 2006.
- [9] A. M. Panindre, K. H. Chang, T. Weirich, and G. S. Frankel, "Technical Note: Syringe Cell for Electrochemical Testing," *CORROSION*, vol. 74, no. 8, pp. 847–850, Aug. 2018, doi: 10.5006/2847.
- [10] "ASTM G61-86 (Reapproved 2018) Standard Test Method for Conducting Cyclic Potentiodynamic Polarization Measurements for Localized Corrosion Susceptibility of Iron-, Nickel-, or Cobalt-Based Alloys." ASTM International, 2018.
- [11] N. Sridhar and G. A. Cragnolino, "Applicability of Repassivation Potential for Long-Term Prediction of Localized Corrosion of Alloy 825 and Type 316L Stainless Steel," CORROSION, vol. 49, no. 11, pp. 885– 894, Nov. 1993, doi: 10.5006/1.3316014.
- [12] D. S. Dunn, G. A. Cragnolino, and N. Sridhar, "An Electrochemical Approach to Predicting Long-Term Localized Corrosion of Corrosion-Resistant High-Level Waste Container Materials," *CORROSION*, vol. 56, no. 1, pp. 90–104, Jan. 2000, doi: 10.5006/1.3280526.
- [13] S. Esmailzadeh, M. Aliofkhazraei, and H. Sarlak, "Interpretation of Cyclic Potentiodynamic Polarization Test Results for Study of Corrosion Behavior of Metals: A Review," *Prot Met Phys Chem Surf*, vol. 54, no. 5, pp. 976–989, Sep. 2018, doi: 10.1134/S207020511805026X.
- [14] "AWS C5.6 Recommended Practices For Gas Metal Arc Welding." American Welding Society, 1989.
- [15] "AWS D18.1/D18.1M:2020 Specification For Welding Of Austenitic Stainless Steel Tube And Pipe Systems In Sanitary (Hygienic) Applications." American Welding Society, 2020.